Electron surface layer at the interface of a plasma and a dielectric wall

R. L. Heinisch, F. X. Bronold, and H. Fehske

Institut für Physik, Ernst-Moritz-Arndt-Universität Greifswald, 17489 Greifswald, Germany

We study the plasma-induced modifications of the potential and charge distribution across the interface of a plasma and a dielectric wall. For this purpose, the wall-bound surplus charge arising from the plasma is modeled as a quasistationary electron surface layer in thermal equilibrium with the wall. It satisfies Poisson's equation and minimizes the grand canonical potential of wall-thermalized excess electrons. Based on an effective model for a graded interface taking into account the image potential and the offset of the conduction band to the potential just outside the dielectric, we specifically calculate the modification of the potential and the distribution of the surplus electrons for MgO, SiO_2, and Al_2O_3 surfaces in contact with a helium discharge. Depending on the electron affinity of the surface, we find two vastly different behaviors. For negative electron affinity, electrons do not penetrate into the wall and a quasi-two-dimensional electron gas is formed in the image potential, while, for positive electron affinity, electrons penetrate into the wall and a negative space-charge layer develops in the interior of the dielectric. We also investigate how the non-neutral electron surface layer—which can be understood as the ultimate boundary of a bounded gas discharge—merges with the neutral bulk of the dielectric.

I. INTRODUCTION

Macroscopic objects in contact with an ionized gas acquire a negative charge because the influx of electrons from the plasma outruns the influx of ions. The collection of electrons at the wall (the boundary of the object) gives rise to a repulsive Coulomb potential which reduces the electron influx until the wall charge reaches a quasistationary value. As a consequence of the electron accumulation at the wall, an electron depleted region, the plasma sheath, is formed adjacent to the wall.

Most of the voltage driving the discharge drops across the sheath. Wall charges may however affect not only the spatial structure of the plasma but also surface-supported elementary processes such as electron-ion recombination and secondary electron emission, which are particularly important in dusty plasmas,[1–3] dielectric barrier discharges,[4–6] and solid-state-based microdischarges.[7–11] A macroscopic description of the plasma-induced wall charge, sufficient for the modeling of the plasma sheath,[12] is clearly insufficient for quantifying the effect wall charges might have on these processes. A microscopic description of the plasma-induced wall charge and the potential across the plasma-wall interface it leads to is required.

Traditionally, plasma walls are treated as perfect absorbers.[12–14] Irrespective of the microscopic interaction, all electrons and ions impinging on the wall are assumed to recombine instantly. From this model, only the wall potential just outside the wall can be obtained. This is the potential that balances the electron and ion influx at the wall. A first, qualitative step going beyond this model was taken by Emeleus and Coulter,[15,16] who envisaged the wall charge as a two-dimensional surface plasma coupled to the bulk plasma via electron-ion wall recombination. No attempt was however made to put this appealing idea onto a formal basis. Later the notion of a two-dimensional surface charge was developed further by Behnke and coworkers[17–19] utilizing phenomenological rate equations for the electron and ion surface densities. In these equations, the microphysics at the

wall is encapsulated in surface parameters, such as electron and ion sticking coefficients, electron and ion desorption times, and an electron-ion wall recombination coefficient. In principle these parameters can be calculated. Assuming, for instance, plasma electrons to adsorb and desorb in the long-range image potential of the wall, we calculated in our previous work electron sticking coefficients and electron desorption times for uncharged metallic[20] and dielectric surfaces.[21–23] We also made a first attempt to estimate these two quantities for charged dielectric plasma walls[24] and proposed a physisorption-inspired microscopic charging model for dust particles in a gas discharge.[25]

In this work, we shift gears and focus on the potential and charge distribution across the plasma-wall interface after the quasistationary wall charge (the electron adsorbate in the notation of our previous work[20–25]) has been established. In other words, we extend the modeling of the plasma sheath[12–14] to the region inside the solid and calculate the plasma-induced modifications of the potential and charge distribution of the surface. Although knowing the potential and charge distribution across the interface may not be of particular importance for present day technological plasmas, it is of fundamental interest from an interface physics point of view. In addition, considering the plasma wall as an integral part of the plasma sheath may become critical when the miniaturization of solid-state-based plasma devices[7–11] continues.

In the model outlined below we specifically consider a dielectric wall and treat the plasma-induced quasistationary wall charge, that is, the surplus charge on top of the charge distribution of the bare, free-standing surface, as an electron surface layer (ESL) of a certain extent, which is trapped by and in thermal equilibrium with the wall. In order to determine the chemical potential, width, and spatial position (relative to the crystallographic interface) of the electron surface layer, which depend on surface as well as plasma parameters, we employ a one-dimensional model for a graded interface between a collisionless plasma sheath and a dielectric surface which is assumed to be a perfect absorber; that is,

the wall potential balances at a certain distance from the crystallographic interface the electron and the ion influx from the plasma.

The model of a graded interface encompasses two important ingredients: the surface dipole of the bare surface responsible for the offset of the conduction-band minimum to the potential just outside the dielectric and the long-range image potential. The former accounts for the charge redistribution of the free-standing, uncharged surface arising from the truncation of the crystal, and the latter supports polarization-induced external surface states (image states), first predicted for liquid helium[26] and later studied for metallic and dielectric surfaces with negative electron affinity,[27–32] which may trap the electron surface layer in front of the crystallographic interface.

Originally proposed by Stern for the interface between two dielectrics,[33] and later used by others for semiconductor heterojunctions[34] and electron trapping in nanopores,[35] the graded interface model also guarantees continuity of the electrostatic potential across the plasma-wall interface. The model thus allows us to study the spatial distribution of the plasma-induced wall charge across the interface. To insert the surplus charge into the interface we follow Tkharev and Danilyuk[36] and minimize, in the spirit of density-functional theory,[37–39] the grand canonical potential of wall-thermalized excess electrons. We also investigate how the electron surface layer merges with the neutral bulk of the dielectric which we describe with the model of an intrinsic semiconductor.

Various improvements of the model are conceivable but the increased mathematical complexity would mask the general ideas we would like to convey. For instance, the model of a collisionless sheath could be replaced by more realistic models.[12–14] Going beyond the perfect absorber model, on the other hand, is an unsolved problem. It would require the inclusion of electron desorption, electron sticking, and electron-ion recombination, with the respective coefficients to be self-consistently calculated for the quasistationary electron adsorbate at the wall. Replacing the graded interface by an *ab initio* theory for the surface, for instance, along the lines given in Refs. [27,28,40] and [41], possibly taking adlayers of the host gas's atoms or molecules as well as impurities and imperfections into account, is desirable but at the present stage of the investigation impractical. It would require an expensive atomistic characterization of the plasma-wall interface, either experimentally via various surface diagnostics or theoretically via *ab initio* simulations. As long as the atomistic details affect however only the offsets of the dielectric constant, the electron affinity, and the effective mass, the graded interface model already incorporates these details by a suitable parametrization. What is not well described is the nonuniversal region a few atomic units below and above the crystallographic interface. In particular, intrinsic surface states (Shockley and Tamm states[42]) and additional surface states which may arise from the short-range surface potential due to impurities, imperfections, and adlayers are not included. If unoccupied these states could trap the electron surface layer in the vicinity of the interface, even for surfaces with positive electron affinity where image states are absent and cannot trap the surplus charge in front of the surface.

The remaining paper is structured as follows. In Sec. II we first construct a crude model for the plasma-induced electron surface layer at the interface between a plasma and a dielectric wall. It does not account for the merging of the electron surface layer with the bulk of the dielectric. As long as the primary interest is in the region close to the crystallographic interface and the band gap of the dielectric is large enough, the crude model is sufficient. Section III describes a refinement of the model which enables one to also investigate the crossover of the electron surface layer to the bulk of the dielectric. This is particularly important for dielectrics with small energy gaps. Numerical results for the potential and the electron distribution are given in Sec. IV, and a short summary is formulated in Sec. V.

II. CRUDE ELECTRON SURFACE LAYER

As depicted in Fig. 1, we consider an ideal, planar interface at $z = 0$ with the dielectric occupying the half space $z < 0$ and the discharge occupying the half space $z > 0$. Chemical contamination and structural damage due to the burning gas discharge are discarded. At the moment we focus on the physical principles controlling the electronic properties of the plasma-wall interface. In the model we propose the plasma-induced wall charge to be treated as an ESL, which is an interface-specific electron distribution on top of the charge redistribution due to the truncation of the solid. The ESL is assumed to be thermalized with the solid and to stretch from the plasma sheath over the crystallographic interface to the bulk of the dielectric.

The boundary between the ESL and the plasma sheath is located in front of the surface at $z = z_0$. It is the position where the attractive force due to the surface potential ϕ_{surf} and the
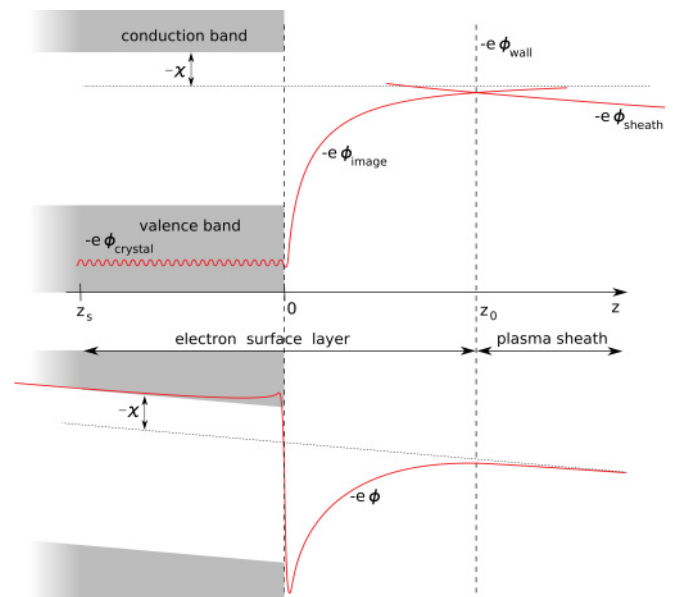

FIG. 1. (Color online) Qualitative sketch of an interface between a plasma and a dielectric wall. Upper panel: band structure, microscopic crystal potential merging with the image potential, and sheath potential. Lower panel: effective potential for the graded interface on which the model of an electron surface layer is based.

repulsive force due to the sheath potential ϕ_{sheath} balance each other. Thus, z_0 is given by

$$\phi'_{\text{surf}}(z_0) + \phi'_{\text{sheath}}(z_0) = 0. \tag{1}$$

It gives the position of an effective wall for plasma electrons and ions at which, for instance, the flux balance condition of the perfect absorber model, $j_e = j_i$, with j_e and j_i, respectively, being the electron and ion flux toward the dielectric surface, has to be fulfilled. For $z < z_0$ an electron is attracted to the surface and thus contained in the ESL, while for $z > z_0$ it is repelled back into the plasma. On the solid side, for $z < 0$, the ESL is bounded because of the shallow potential well formed by the restoring force from the positive charge in the plasma sheath.

In this section we will outline the essential building blocks of the ESL model. Putting together concepts from plasma as well as surface physics, a detailed, self-contained account seems to be helpful.

A. Plasma sheath

In the traditional view, electrons missing in the positive space-charge region (SCR) in front of the plasma wall accumulate on the wall and give rise to a wall potential. For the construction of our one-dimensional interface model we need the total number per unit area of missing sheath electrons (that is, the total surface density of missing sheath electrons) as a function of the wall potential because it is this number of electrons which can be distributed across the ESL. Hence, we require a model for the plasma sheath.

For simplicity, we use a collisionless sheath;[12] more realistic sheath models[12–14] make no difference in principle. In the collisionless sheath, electrons are thermalized, that is, the electron density $n_e = n_0 \exp(e\phi/k_B T_e)$, with ϕ being the potential, n_0 being the plasma density, and T_e being the electron temperature. The ions enter the sheath with a directed velocity v_{i0} and satisfy a source-free continuity equation, $d(n_i v_i)/dz = 0$, implying $n_i v_i = n_0 v_{i0}$, and an equation of motion $M(v_i \frac{d}{dz} v_i) = -e \frac{d}{dz}\phi$, with n_i being the ion density and M being the ion mass. The potential ϕ satisfies Poisson's equation $d^2\phi/dz^2 = -4\pi e(n_i - n_e)$. Thus, the governing equations for the collisionless plasma sheath are[12]

$$v_i \frac{dv_i}{dz} = -\frac{e}{M}\frac{d\phi}{dz} \quad \text{and} \tag{2}$$

$$\frac{d^2}{dz^2}\phi = -4\pi e n_0 \left[\frac{v_0}{v_i} - \exp\left(\frac{e\phi}{k_B T_e}\right) \right]. \tag{3}$$

Using dimensionless variables

$$\eta = -\frac{e\phi}{k_B T_e}, \quad \xi = \frac{z}{\lambda_D}, \quad \text{and} \quad u = \frac{v_i}{c_s}, \tag{4}$$

where

$$\lambda_D = \sqrt{\frac{k_B T_e}{4\pi n_0 e^2}} \quad \text{and} \quad c_s = \sqrt{\frac{k_B T_e}{M}}, \tag{5}$$

Eqs. (2) and (3) become

$$uu' = \eta' \quad \text{and} \tag{6}$$

$$\eta'' = \frac{u_0}{u} - \exp(-\eta). \tag{7}$$

In the ESL model the plasma occupies not the whole half space $z > 0$ but only the portion $z > z_0$ (see Fig. 1). The integration of the first equation gives $u = -\sqrt{2\eta + u_0^2}$, where $u_0 = v_{i0}/c_s$ is the reduced velocity of ions entering the sheath, so that the second equation becomes

$$\eta'' = -\frac{u_0}{\sqrt{2\eta + u_0^2}} - \exp(-\eta). \tag{8}$$

Using the boundary condition that the potential and the field vanish far inside the plasma, that is, $\eta \to 0$ and $\eta' \to 0$ for $\xi \to \infty$, Eq. (8) can be integrated once and we obtain

$$\eta' = -\sqrt{-2u_0\sqrt{2\eta + u_0^2} + 2\exp(-\eta) + 2u_0\sqrt{u_0^2} - 2}. \tag{9}$$

For ions entering the sheath with the Bohm velocity, $u_0 = -1$. The field at the wall as a function of the wall potential $\eta_w = \eta(\xi_0)$ is then given by

$$\eta'_w = -\sqrt{2\sqrt{2\eta_w + 1} + 2\exp(-\eta_w) - 4}. \tag{10}$$

The total surface density of electrons in the ESL equals the total surface density of missing sheath electrons, in other words, the total surplus surface density of positive ions in the sheath N which can be calculated from the electric field at the wall. Integrating Poisson's equation yields

$$N = \int_{z_0}^{\infty} dz(n_i - n_e) = -\frac{1}{4\pi e} \int_{z_0}^{\infty} dz \frac{d^2\phi}{dz^2}$$

$$= \frac{1}{4\pi e}\frac{d\phi}{dz}(z_0) = -n_0 \lambda_D \eta'_w. \tag{11}$$

Combing Eqs. (11) and (10) gives the total surface density of electrons to be inserted into the ESL as a function of the wall potential.

The wall potential itself is determined by the flux balance condition, $j_e = j_i$, which, in the ESL model, is assumed to be fulfilled at $z = z_0$. Using the Bohm flux for the ions and the thermal flux for the electrons,

$$j_i = n_0 \sqrt{\frac{k_B T_e}{M}} \quad \text{and} \quad j_e = \frac{1}{4} n_0 \sqrt{\frac{8 k_B T}{\pi m_e}} e^{\frac{e\phi}{k_B T_e}}, \tag{12}$$

the wall potential is given by[12]

$$\eta_w = \frac{1}{2}\ln\left(\frac{M}{2\pi m_e}\right), \tag{13}$$

that is,

$$\phi_w = -\frac{k_B T_e}{2e}\ln\left(\frac{M}{2\pi m_e}\right). \tag{14}$$

In the collisionless sheath model the wall potential depends only on the electron temperature and the ion to electron mass ratio.

B. Surface dipole

We now turn to the interface region in which the missing sheath electrons will be inserted. This region is absent in the traditional modeling of plasma walls. In our model it is an extended region surrounding an ideal dielectric surface.

In comparison to the electrons responsible for the chemical binding within the dielectric the additional electrons coming from the plasma are only a few. The electronic structure of the surface, in particular, the charge redistribution due to truncation of the solid and the offset of the energy bands in the bulk with respect to the potential outside the dielectric, will not be changed significantly by the presence of the surplus electrons comprising the wall charge.

In order to quantify the above statement let us first consider the electrostatic potential and the electronic structure of a freestanding, uncharged dielectric surface. According to Tung,[43] it has to minimize the thermodynamical potential and satisfy Poisson's equation, implying that the potential is continuous across the surface. Strictly speaking, the continuity of the potential only applies to the microscopic crystal potential which has to merge continuously with the surface potential outside the crystal. The averaged long-range potential, in contrast, can be discontinuous at the interface. It is this offset which is encoded in the surface dipole.

The energy of an electronic state in the bulk of the dielectric can be referenced to the vacuum level $V(\infty) = 0$, that is, the potential far outside the crystal, in the following way:[43]

$$E_{ik}(\vec{r}) = \epsilon_{ik} - e\bar{V}_{\text{cell}} - eV_s(\vec{r}), \qquad (15)$$

where ϵ_{ik} is the quantum-mechanical contribution to the energy, $\bar{V}_{\text{cell}}$ is the averaged potential of a cell due to the charge distribution within the same cell, and $V_s(\vec{r})$ is the long-range potential due to the surface dipole, space charges, and external fields. In the simple two-band model depicted in Fig. 1, $i = v,c$. $V_s(\vec{r})$ contains the surface dipole arising from the truncation of the solid and responsible for the potential offset at the surface and a slowly varying component due to external fields and internal and plasma-induced space charges. External fields and internal space charges will be neglected in the following, and plasma-induced space charges will be accounted for by Poisson's equation (see below).

In order to judge whether the surplus charge arising from the plasma affects the surface dipole it is useful to consider first the typical strength of the surface dipole of a free-standing, uncharged dielectric surface. It results from a charge double layer in immediate proximity to the surface. Depending on the material it can have various origins. For an ionic crystal, for example, it is the lattice relaxation at the surface which makes anions or cations protrude and the other species retract (e.g., protruding oxygen and retracted cations for magnesium oxide[27]), while for semiconductors it is the regrouping of covalent bonds which leads to charge redistribution at the surface. Even in the absence of these effects the minimization of the thermodynamic potential of the surface's electrons leads already to an electron density leaking out into the vacuum. This is particularly important for metals. As a result a charge double layer is formed over a length on the order of a lattice constant.

The dipole layer is usually characterized by a dipole strength:

$$eD = eV_s(\vec{r}_s^-) - eV(\vec{r}_s^+), \qquad (16)$$

where $V_s(\vec{r}_s^-)$ is the limit of the long-range potential just inside the crystal at the surface position $\vec{r}_s$ and $V(\vec{r}_s^+)$ is the limit of

the potential at that position just outside the surface. Usually these two potentials, which characterize the discontinuity of the long-range potential at the surface, are termed the potential just inside and the potential just outside, respectively.[43,44] Here, just outside denotes a distance that is small compared to variations of the long-range potential due to external fields or space charges but large compared with the width of the charge double layer. Note also that, in the definition of the potential just outside the image potential is assumed to have already decreased to zero.[44] This point will be important later.

The strength of the dipole layer is a microscopic property of the surface which is relatively insensitive against the additional charges from the plasma. The reason for this lies in the small number of additional electrons from the plasma compared to the number of displaced electrons involved in the formation of the dipole layer. To prove this statement we give a simple estimate. Typical surface dipoles eD are on the order of electron volts. For a double layer of 1 Å to each side of the crystallographic interface a potential difference of 1 V requires a surface charge density of $5.5 \times 10^{13} \text{cm}^{-2}$. The surface charge density at the wall of a helium discharge with plasma density $n_0 = 10^7 \text{cm}^{-3}$ and electron temperature $k_B T_e = 2 \text{eV}$ amounts, however, only to $4.4 \times 10^6 \text{cm}^{-2}$. For typical plasma densities, the number of additional electrons is thus far too small to lead to a change of the surface dipole. Even for semiconductor-based microdischarges,[8,10] which can have much higher plasma densities, we expect the surface dipole of the plasma wall not to be modified by the plasma.

In view of the preceding estimate, we have to revise an assumption in our previous work,[23] where we assumed the surface charge accumulating on the wall would increase the dipole energy eD by $e\phi_w$, leading to the image states being pushed from the band gap into the energy region of the conduction band. The numbers given in the previous paragraph indicate, however, that the band lineup of the conduction band and the potential just outside the solid will not be affected much by the wall charge. Hence, if a negative electron affinity supports image states in front of the uncharged surface, these states remain in the band gap for the charged surface. Electron trapping as investigated in Refs. 21 and 22 is thus possible even for charged plasma walls.

Instead of the dipole strength eD which cannot be measured directly, it is more convenient to characterize the dipole layer by the electron affinity χ which is a measurable quantity for a dielectric surface.[44] The electron affinity is the energy released when an electron is moved from just outside the surface to the bottom of the conduction band. It accounts for charge redistribution in the vicinity of the surface due to the truncation of the crystal. While many surfaces have positive electron affinity such as Al_2O_3 or SiO_2, there are also materials with negative electron affinity, for instance, diamond,[45] boron nitride,[46] or the alkaline earth oxides.[27,28] The electron affinity depends also on adatoms. In some cases this is even used to control the electron affinity of a surface. Terminating, for instance, a surface with weakly electronegative elements such as hydrogen induces a negative electron affinity,[47] while termination with strongly electronegative elements can lead to a positive electron affinity.[48]

From Eq. (15) it is clear that χ equals eD plus a bulk contribution:

$$\chi = -eV_s(\vec{r}_s^+) - E_{ck}(\vec{r}_s^-) = eD - E_C + e\bar{V}_{\text{cell}}, \quad (17)$$

where $E_C = \epsilon_{\text{cm}}$ denotes the minimum of the conduction band. We can thus use χ to characterize the potential offset at the surface. There is however a caveat. The long-range potential inside the solid is only specified up to a constant.[43] Typical choices are the cell-averaged potential or the intersphere potential of the muffin-tin approximation. For our purpose it will be however more convenient to take the conduction-band minimum as the long-range potential inside the solid. This choice is motivated as follows. We are considering a dielectric with a large energy gap. The valence band is thus fully occupied and the conduction band is essentially empty. Hence, only the conduction band can be populated by additional electrons coming from the plasma, and referencing the electrostatic potential inside the solid to the conduction-band minimum allows us to relate the total surplus electron density in the interface region to the potential in the interface region, in analogy to what we have done for the plasma sheath in the previous subsection.

Adopting the above discussion to the one-dimensional model shown in Fig. 1 and assuming a quadratic dispersion for the conduction band, the energy of an electron in the conduction band is given by

$$E_k(z) = \frac{\hbar^2 k^2}{2m_C^*} - e\phi_{\text{surf}}(z), \quad (18)$$

where $\phi_{\text{surf}}(z)$ is the total surface potential to be determined in the next subsection, and the offset of the electrostatic potential at the surface,

$$e\phi_{\text{surf}}(0^-) - e\phi_{\text{surf}}(0^+) = \chi, \quad (19)$$

encompasses the surface dipole as well as the unspecified bulk contribution.

C. Image potential

The surface potential of the bare, uncharged surface comprises at least the surface dipole and a long-range contribution, the image potential, resulting from the mismatch of the dielectric constants at the surface. Far away from the surface the image potential is given by[49]

$$\phi_{\text{im}}(z) = \frac{\epsilon - 1}{4(\epsilon + 1)} \frac{e}{z}. \quad (20)$$

But this expression cannot be employed for our purpose because the singularity at $z = 0$ prohibits a smooth electron distribution across the interface. In reality the image potential has to continuously merge with the crystal potential. Equation (20) is thus also unphysical.

To obtain a realistic image potential without performing an atomistically accurate calculation we employ the model of a graded interface. It also has the virtue of being parameterizable with experimentally measured values for the electron affinity,

the dielectric mismatch, and the mismatch between effective electron masses. The model incorporates therefore important properties of a surface; most importantly, it accounts for the charge redistribution due to the truncation of the solid.

Initially proposed by Stern[33] to remove the unphysical singularity of the image potential at the interface of two dielectrics, the graded interface model assumes the dielectric constant ϵ to vary over a distance on the order of a lattice constant. Later the model was extended to variations of other physical quantities and applied to semiconductor heterostructures and nanopores.[34,35] Clearly, because of the interpolation the model cannot account for effects associated with intrinsic surface states (Shockley and Tamm states[42]) and additional surface states which may arise from the short-range surface potential. Nevertheless, the graded interface model is a reasonable description of a surface.

In the spirit of a graded interface, we assume the dielectric constant ϵ, the electron mass m, and the potential offset at the surface to vary smoothly according to the grading function

$$g_{c^-,c^+}(z) = \begin{cases} c^- & z < -a \\ \frac{c^- + c^+}{2} - \frac{c^- - c^+}{2}\sin\left(\frac{\pi x}{2a}\right) & -a < z < a, \\ c^+ & z > a \end{cases} \quad (21)$$

where a is the half width of the graded interface and $c^\mp$ stands for the quantity that varies across the interface. We use the value $a = 5$ Å, which is an estimate used in previous applications of the graded interface.[33–35] While the grading parameter a is not based on definite experimental or theoretical results it is motivated by the assumption that the bonding and the electron density at the surface change over one to two lattice constants, implying a transition layer for the effective potential and the dielectric constant that is somewhat larger. Hence, across the interface the electron mass, the dielectric constant, and the offset potential are given by

$$m(z) = g_{m_C^*,m_e}(z), \quad \epsilon(z) = g_{\epsilon,1}(z), \quad (22)$$

and

$$\phi_{\text{offset}}(z) = \frac{1}{e} g_{\chi,0}(z), \quad (23)$$

respectively, with m_C^* being the effective mass of the conduction band.

Within the model of the graded interface, the image potential is the change in the self-energy of an electron due to the proximity of the dielectric mismatch. Positioning the electron at $\vec{r}_0$ it is given by[33]

$$\phi_{\text{im}}(\vec{r}_0) = \frac{1}{2}[\phi^m(\vec{r}_0) - \phi^0(\vec{r}_0)], \quad (24)$$

where $\phi^m(\vec{r})$ is the potential in the medium with dielectric mismatch arising from the electron at $\vec{r}_0$ and $\phi^0(\vec{r})$ is the same quantity in a homogeneous medium with dielectric constant $\epsilon(z_0)$. Hence, $\phi^m(\vec{r})$ is the solution of

$$\nabla[\epsilon(z)\nabla\phi^m(\vec{r})] = 4\pi e\delta(\vec{r} - \vec{r}_0), \quad (25)$$

while $\phi^0(\vec{r})$ is the solution of

$$\nabla^2\phi^0(\vec{r}) = \frac{4\pi e}{\epsilon(z_0)}\delta(\vec{r} - \vec{r}_0). \quad (26)$$

To solve Eqs. (25) and (26) we follow Stern[33] and make the ansatz

$$\phi^{m,0}(z,\rho,\phi) = \frac{1}{2\pi} \sum_{l=-\infty}^{\infty} \int_0^\infty dq\, q\, J_l(\rho q) J_l(\rho_0 q)$$
$$\times e^{il(\phi-\phi_0)} A_q^{m,0}(z). \quad (27)$$

Placing the electron on the z axis, $\rho_0 = 0$, which implies $J_0(\rho_0 q) = 1$ and $J_l(\rho_0 q) = 0$ for $l > 0$. Hence, we need to keep only the $l = 0$ term, so that

$$\phi^{m,0}(z,\rho,\phi) = \frac{1}{2\pi} \int_0^\infty dq\, q\, J_0(\rho q) A_q^{m,0}(z), \quad (28)$$

where $A_q^0(z)$ is given by

$$A_q^0(z) = \frac{-2\pi e}{\epsilon(z_0)q} e^{-q|z-z_0|} \quad (29)$$

and $A_q^m(z)$ is the solution of

$$A_q^{m''}(z) + \frac{\epsilon'(z)}{\epsilon(z)} A_q^{m'}(z) - q^2 A_q^m(z) = \frac{4\pi e}{\epsilon(z)} \delta(z - z_0), \quad (30)$$

which has to be obtained numerically. The image potential is then given by

$$\phi_{\text{im}}(z_0) = \frac{1}{4\pi} \int_0^\infty dq\, q \big[A_q^m(z_0) - A_q^0(z_0) \big]. \quad (31)$$

In contrast to Eq. (20) it is now smoothly varying across the interface with a deep well on the low-ϵ side and a small bump on the high-ϵ side.

The total surface potential comprises the graded offset potential Eq. (23) and the graded image potential. Hence,

$$\phi_{\text{surf}}(z) = \phi_{\text{im}}(z) + \phi_{\text{offset}}(z). \quad (32)$$

It is continuous across the crystallographic interface at $z = 0$ and enables us thereby to also calculate a smoothly varying electron distribution in the ESL. The band structure and the total surface potential at the graded interface are visualized in the lower panel of Fig. 1.

Using Eq. (1) we can now determine the position z_0 of the effective wall, that is, the maximum extent of the ESL on the plasma side. The derivative of the bare surface potential is $\phi'_{\text{surf}} = \phi'_{\text{offset}} + \phi'_{im}$. Due to the relatively weak field in the sheath compared to the image force, the boundary z_0 will be so far away from the interface that ϕ'_{offset} vanishes and the image potential obeys Eq. (20). Thus, the boundary between the ESL and the plasma sheath is given by

$$z_0 = \sqrt{\frac{(\epsilon - 1)e}{4(\epsilon + 1)\phi'_w}}, \quad (33)$$

with $\phi'_w = -(k_B T_e \eta'_w)/(e\lambda_D)$ and η'_w given by Eq. (10).

D. Electron distribution

The plasma-induced wall charge is assumed to be in thermal equilibrium with the wall. Hence, the distribution of the excess electrons in the ESL has to minimize the excess electron's grand canonical potential in the external potential due to the surface. The coupling to the sheath is maintained by the constraint that only as many electrons can be filled into the

ESL as are missing in the sheath and the boundary conditions to the Poisson equation, which links the electron distribution in the ESL to the (internal) electrostatic potential.

To minimize the grand canonical potential of the surplus electrons we follow Tkharev and Danilyuk[36] and apply density-functional theory[37,38] to the graded interface. While more refined schemes of density-functional theory[39] could, in principle, be employed, we will use for the purpose of this exploratory calculation density-functional theory in the local approximation. Quite generally, the grand canonical potential of an electron system in an external potential $V(\vec{r})$ is given in the local approximation by

$$\Omega = \int V(\vec{r})n(\vec{r})d\vec{r} - \frac{e}{2} \int \phi_C(\vec{r})n(\vec{r})d\vec{r}$$
$$+ G[n] - \mu \int n(\vec{r})d\vec{r}, \quad (34)$$

where $G[n]$ is the grand canonical potential of the homogeneous system with density $n(\vec{r})$ and the Coulomb potential is determined by

$$\nabla[\epsilon(\vec{r})\nabla\phi_C(\vec{r})] = 4\pi e n(\vec{r}). \quad (35)$$

The ground-state electron density minimizes Ω; that is, it satisfies

$$V(\vec{r}) - e\phi_C(\vec{r}) + \mu^h(n) - \mu = 0, \quad (36)$$

where $\mu^h(n) = \delta G[n]/\delta n$ is the chemical potential for the homogeneous system.

Specifically for the excess electrons in the one-dimensional graded interface Eq. (36) reduces to

$$-e\phi(z) + \mu^h(z) - \mu = 0, \quad (37)$$

where $\mu^h(z) \equiv \mu^h[n(z),T]$ and the electrostatic potential,

$$\phi(z) = \phi_{\text{surf}}(z) + \phi_C(z), \quad (38)$$

consists of the potential of the bare surface given by Eq. (32) and the internal Coulomb potential which satisfies Poisson's equation:

$$\frac{d}{dz}\left[\epsilon(z)\frac{d}{dz}\phi_C(z)\right] = 4\pi e n(z), \quad (39)$$

with the graded dielectric constant $\epsilon(z)$ given by Eq. (22) and the boundary conditions $\phi_C(z_0) = \phi_w$ and $\phi'_C(z_0) = \phi'_w$ to guarantee continuity of the potential at z_0 and to include the restoring force from the positive charge in the sheath. Note that the Coulomb potential derived from this equation includes the attraction of an electron to the image of the charge distribution.

For the functional relation $\mu^h(z) \equiv \mu^h[n(z),T]$ we take the expression adequate for a homogeneous, noninteracting, nondegenerate electron gas:

$$n(z) = \frac{1}{\sqrt{2}}\left[\frac{m(z)kT}{\pi\hbar^2}\right]^{\frac{3}{2}} e^{\frac{\mu^h(z)}{k_B T}}. \quad (40)$$

This is justified because the density of the excess electrons is rather low and the temperature of the surface is rather high, typically a few hundred Kelvins.

In order to calculate the quasistationary distribution of the surplus electrons, Eqs. (37) and (39) have to be solved self-consistently with the additional constraint that the total

electron surface density in the ESL equals the total surface density of electrons missing in the sheath, that is,

$$\int_{z_s}^{z_0} dz\, n(z) = N, \qquad (41)$$

with N given by Eq. (11). In the above equation we introduced a cutoff $z_s < 0$ at which the ESL terminates inside the dielectric. As long as $|z_s|$ is chosen large enough it does not affect the numerical results close to the surface. An improved treatment of the ESL, avoiding the *ad hoc* cutoff, is given in the next section.

Within the crude ESL model developed in this section the computation is performed iteratively in the interval $z_s < z < z_0$ according to the following scheme:

(i) We start with the potential of the empty surface given by Eq. (38) with $\phi_C(z)$ obtained from Eq. (39) with $n(z) = 0$ but with the boundary conditions at z_0 as specified.

(ii) We integrate both sides of Eq. (40) over z with $\mu^h(z)$ given by Eq. (37). Enforcing the constraint (41) determines μ.

(iii) Using μ we calculate from Eq. (37) a new $\mu^h(z)$ which gives with Eq. (40) a new electron density $n(z)$.

(iv) Lastly, we determine from Eq. (39) the electrostatic potential associated with the updated $n(z)$.

Steps (ii)–(iv) are iterated until μ, which is far below the conduction-band edge because of the nondegeneracy of the excess electrons, converges.

III. REFINED ELECTRON SURFACE LAYER

In the previous section we have taken into account only the electron concentration in the conduction band of the dielectric due to the electrons coming from the plasma. For wide band-gap materials this is justified, especially near the surface, as their concentration is much larger than the intrinsic carrier concentration. Deep inside the dielectric, however, charge neutrality is not enabled by a vanishing electron density but by the electron density decreasing to its intrinsic value, which is then balanced by the intrinsic hole concentration in the valence band.

To take this effect into account, which is particularly important when the additional electrons accumulate deep inside the bulk of the dielectric, we divide the ESL into two regions: a very narrow interface-specific region (ISR) and a wide space-charge region (SCR) in the bulk of the dielectric. The parameter z_s denotes now no longer an *ad hoc* cutoff but the boundary between the two regions. It has to be chosen so that the ISR includes the major effect of the image potential in the dielectric implying $z_s < -z_0$. The electron distribution and the potential in the ISR are calculated using the density-functional approach outlined in the previous section. In the SCR we use for simplicity the model of an intrinsic semiconductor to describe electron and hole densities as well as the long-range potential. As the energy bands in the dielectric follow the long-range potential the refined ESL also captures the band bending which might be induced by the presence of the wall charge. It is however only significant when most of the excess electrons are trapped in the SCR and not in the ISR.

Figure 2 schematically shows the electron and hole densities for the refined ESL model. The boundary between the plasma
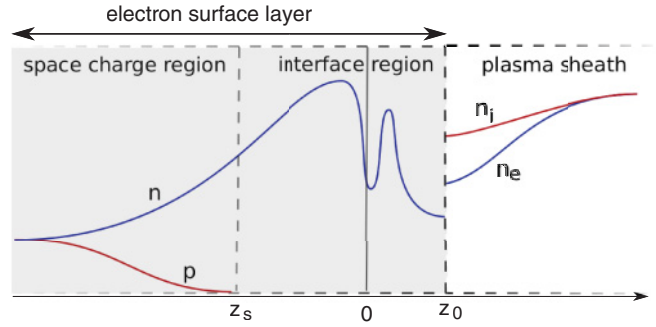

FIG. 2. (Color online) Sketch of the refined model of the interface between a plasma and a dielectric wall. In the plasma, equal densities of electrons and ions ensure quasineutrality. The positive space charge in front of the effective wall defines the plasma sheath. The ESL contains a very narrow interface-specific region (ISR), where the model of the graded interface is used, and a wide space-charge region (SCR), which allows a continuous merging with the neutral bulk of the dielectric, where intrinsic electrons and holes balance each other to guarantee charge neutrality. Note that the widths of the various regions are not to scale.

sheath and the ESL is still located at z_0. As our model does not encompass the electron and ion flux from the plasma for $z < z_0$, the densities n_e and n_i are discontinuous at z_0. This is obvious for the ions which are not allowed to enter the solid. The discontinuity of the electron density, in contrast, arises because we ensure only the total number of missing sheath electrons per unit area to be conserved. This global constraint cannot guarantee continuity of the electron density at z_0. At the boundary between the ISR ($z_s < z < z_0$) and the SCR ($z < z_s$) the electron density and the potential are continuous. In principle, also the hole density p should be continuous. As $p(z_s) \ll n(z_s)$ for the materials we are considering, we can however neglect holes in the ISR.

For the modeling of the SCR it is convenient to use $\psi(z) = \phi(z) - \phi_{\text{bulk}}$ for the long-range potential, which vanishes for charge neutrality in the bulk. Here, $\phi_{\text{bulk}} = \phi(-\infty)$ (see below for an explicit relation for ϕ_{bulk}). Then, Poisson's equation is given by

$$\frac{d^2\psi(z)}{dz^2} = -\frac{4\pi}{\epsilon}\left[-en(z) + ep(z)\right], \qquad (42)$$

where the electron and hole densities for an intrinsic semiconductor with parabolic bands whose extremal points are, respectively, E_C and E_V are given by[50]

$$n(z) = \frac{1}{\sqrt{2}}\left(\frac{m_C^* k_B T}{\pi \hbar^2}\right)^{\frac{3}{2}} e^{\frac{1}{k_B T}[\nu - E_C + e\psi(z)]}, \qquad (43)$$

$$p(z) = \frac{1}{\sqrt{2}}\left(\frac{m_V^* k_B T}{\pi \hbar^2}\right)^{\frac{3}{2}} e^{-\frac{1}{k_B T}[\nu - E_V + e\psi(z)]}. \qquad (44)$$

From a comparison of the exponents in Eqs. (43) and (40), where μ_h is given by Eq. (37), we find

$$\nu = \mu + E_C + e\phi_{\text{bulk}}. \qquad (45)$$

Far from the surface, $\psi = 0$ and $n = p = n_b$. This gives the chemical potential

$$\nu = \frac{E_V + E_C}{2} + \frac{3}{4} k_B T \ln\left(\frac{m_V^*}{m_C^*}\right) \tag{46}$$

and the bulk carrier concentration

$$n_b = \frac{1}{\sqrt{2}} \left(\frac{k_B T}{\pi \hbar^2}\right)^{\frac{3}{2}} (m_C^* m_V^*)^{\frac{3}{4}} \exp\left(-\frac{E_g}{2k_B T}\right), \tag{47}$$

where $E_g = E_C - E_V$. Hence, Poisson's equation becomes

$$\frac{d^2\psi(z)}{dz^2} = \frac{4\pi e}{\epsilon} n_b \left[e^{\frac{e\psi(z)}{k_B T}} - e^{-\frac{e\psi(z)}{k_B T}}\right], \tag{48}$$

and using dimensionless variables

$$\eta = \frac{e\psi}{k_B T} \quad \text{and} \quad \xi = \frac{z - z_s}{L_D} \tag{49}$$

with $L_D = \sqrt{\epsilon k_B T / 4\pi e^2 n_b}$ we obtain

$$\eta'' = e^\eta - e^{-\eta}. \tag{50}$$

This equation can be integrated once, which gives

$$(\eta')^2 = 4\cosh(\eta) + C. \tag{51}$$

The boundary conditions in the bulk $\eta = 0$ and $\eta' = 0$ for $\xi \to -\infty$ imply $C = -4$ so that Eq. (51) becomes

$$\eta' = \sqrt{8} \sinh\left(\frac{\eta}{2}\right). \tag{52}$$

Integration with the boundary condition at z_s, that is, at $\xi = 0$, $\eta(0) = \eta_s$ and requiring $\eta \to 0$ for $\xi \to -\infty$ gives

$$\eta^\pm(\xi) = \mp 2 \ln\left[\pm \tanh\left(\frac{\mp\xi}{\sqrt{2}} + \frac{c^\pm}{2}\right)\right], \tag{53}$$

with

$$c^\pm = \pm 2 \text{artanh}\left[\exp\left(\frac{\mp\eta_s}{2}\right)\right], \tag{54}$$

where the upper sign is for $\eta_s > 0$ and the lower sign is for $\eta_s < 0$.

In analogy to what we have done at the boundary of the ESL with the plasma sheath at $z = z_0$ we relate the potential η_s to the total electron surface density in the space-charge region. From Poisson's equation we obtain for the total electron surface density in the SCR

$$N^{\text{SCR}} = \int_{-\infty}^{z_s} dz(n - p) = L_D^2 n_b \left.\frac{d\eta}{dz}\right|_{-\infty}^{z_s}$$
$$= L_D n_b \eta'(0), \tag{55}$$

where η' is given by Eq. (52), so that

$$N^{\text{SCR}} = \sqrt{8} L_D n_b \sinh\left(\frac{\eta_s}{2}\right) \tag{56}$$

or

$$\eta_s = 2 \text{arsinh}\left(\frac{N^{\text{SCR}}}{\sqrt{8} L_D n_b}\right). \tag{57}$$

For a negative space charge $\eta_s > 0$, so that the potential is given by $\psi(z) = (k_B T/e)\eta^+[(z - z_s)/L_D]$ and the electron and hole densities are given by $n(z) = n_b e^{\eta^+[(z-z_s)/L_D]}$ and $p(z) = n_b e^{-\eta^+[(z-z_s)/L_D]}$, respectively. The relation between

ψ and ϕ is given by $\phi_{\text{bulk}} = \phi(z) - \psi(z)$. Since $\psi(z_s) = (kT/e)\eta_s$ we obtain $\phi_{\text{bulk}} = \phi(z_s) - (kT/e)\eta_s$.

Now, quite generally, the excess electrons in the ESL are distributed over the ISR and SCR according to

$$N = N^{\text{ISR}}(\mu) + N^{\text{SCR}}(\mu), \tag{58}$$

where N^{ISR} is the surface density of electrons in the ISR, μ is the chemical potential in both regions, and N is the total surface density of missing sheath electrons given by Eq. (11). The total surface density in the ISR is given by $N^{\text{ISR}} = \int_{z_s}^{z_0} dz n(z)$, where $n(z)$ is calculated with the density-functional approach for the graded interface. Requiring continuity of the electron density at z_s,

$$\frac{1}{\sqrt{2}} \left(\frac{m_C^* k_B T}{\pi \hbar^2}\right)^{\frac{3}{2}} e^{\frac{1}{k_B T}[\mu + e\phi(z_s)]} = n_b e^{\eta_s} \tag{59}$$

gives η_s as a function of μ. From η_s we finally obtain, using Eq. (56), $N^{\text{SCR}}(\mu)$.

For the calculation of the electron distribution and the potential in the refined ESL we use the iteration cycle described in the last section with one modification. In step (ii) we solve Eq. (58) instead of Eq. (41) to fix μ. From μ we obtain, using Eq. (59), η_s, which in turn determines the electron distribution and the potential in the SCR. This gives for each iteration step a continuous potential and electron distribution at z_s. As before, the steps (ii)–(iv) are iterated until μ converges.

At the end of this section let us finally mention two simplifications of the refined ESL model, which could be used, respectively, for large band-gap dielectrics irrespective of the electron affinity and dielectrics with small band-gap and positive electron affinity. In the former case the intrinsic carrier concentration n_b is very low and the merger with the bulk occurs very deep in the dielectric. Almost all surplus electrons are however much closer to the surface where the holes can be neglected. This can be seen from the differential equation for η. For small n_b Eq. (57) gives a large η_s. As η satisfies a highly nonlinear differential equation (50), a large η_s implies a steeper gradient of η near the surface so that almost all electrons are concentrated close to the surface where neglecting the holes has little effect. Hence, for large band-gap dielectrics surplus electrons can be filled into a sufficiently large ISR for which the crude ESL model of the previous section will be sufficient provided the cutoff z_s is large enough. The merger with the bulk is of course not correctly captured by such an approach.

For dielectrics or semiconductors with small energy gaps and positive electron affinity, on the other hand, almost all surplus electrons are deep inside the material. It is thus a good approximation to neglect the ISR and to fill all electrons in a SCR. Neglecting the surface potential has little effect in this case and using the SCR already for $z \leqslant 0$ gives a good description of the electron distribution inside the ESL. The electron density and potential at the surface and in front of it can of course not be captured by such an approach. As before $\psi(z) = \phi(z) - \phi_{\text{bulk}}$ with $\phi_{\text{bulk}} = \phi(z_s) - (k_B T/e)\eta_s$ where $\phi(z_s)$ is now the limit of the long-range potential just inside the dielectric given by $\phi(z_s) = \phi_w + \chi/e$.

IV. RESULTS

We now use the ESL model to calculate for a helium discharge in contact with a MgO, Al_2O_3, and SiO_2 surface the potential and the density of excess electrons across the plasma wall. Our main focus lies in the identification of generic types of electron distributions in the ESL depending on plasma and surface parameters. Unless otherwise stated, we use for the plasma density $n_0 = 10^7$ cm^{-3} and for the electron temperature $k_B T_e = 2$ eV. The parameters of the dielectric surfaces are given in Table I. Preferentially we used experimental data for the various quantities; only if not available, we employed theoretical values.[28,51–60]

First we give typical values for z_0, the position where the ESL merges with the plasma sheath. It is calculated from Eq. (1) and should thus depend not only on plasma but also on surface parameters. Our results for MgO ($z_0 = 6.08 \times 10^{-5}$ cm), Al_3O_3 ($z_0 = 6.09 \times 10^{-5}$ cm), and SiO_2 ($z_0 = 5.14 \times 10^{-5}$ cm) indicate however that z_0 is relatively insensitive to ϵ, which is the only surface parameter affecting z_0 when the sheath is assumed to be collisionless. Even the significantly smaller ϵ of SiO_2 does not alter z_0 considerably. For the helium discharge considered z_0 is irrespective of the dielectric always on the order of a micron.

Of particular importance for the distribution of the excess electrons in the ESL is the electron affinity χ, characterizing the offset of the conduction band to the potential just outside. For $\chi < 0$ (MgO) the conduction-band minimum lies above the potential just outside. It is thus energetically favorable for electrons to be located in the image potential in front of the surface. Figure 3, showing the electron density and the potential in the ESL of MgO, verifies this. The energy of an electron in the image potential $-e\phi$ indeed reaches a minimum just in front of the surface at the beginning of the graded interface. For negative electron affinity, the excess electrons coming from the plasma thus form an external surface charge in the image potential in front of the crystallographic interface. The band bending associated with it is negligible. The external surface charge is very narrow; it can thus be considered as a quasi-two-dimensional electron gas, similar to the surface plasma anticipated by Emeleus and Coulter.[15,16]

For $\chi > 0$, on the other hand, the conduction-band minimum is below the potential just outside. It is thus energetically favorable for electrons to accumulate inside the dielectric. This can be seen in Fig. 4, which shows the electron density and the potential in the refined ESL (red line) and simplified ESL (open green circles and blue triangles) for an Al_2O_3 surface. The surface potential consists of an attractive well in front of

TABLE I. Material parameters for the dielectrics considered in this work: dielectric constant ϵ_s, electron affinity χ, conduction-band effective mass m_C^*, valence-band effective mass m_V^*, and band gap E_g.

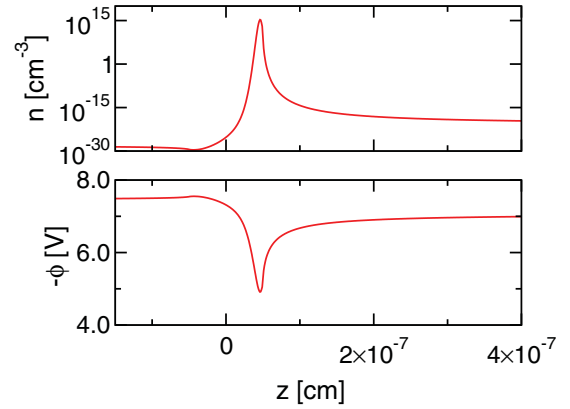|	ϵ_s	χ (eV)	m_C^* (m_e)	m_V^* (m_e)	E_g (eV)
MgO	9.8 [51]	−0.4 [28]	0.4 [52]		
Al_2O_3	9.9 [53]	2.5 [54]	0.4 [55]	4.0 [55]	8.8 [56]
SiO_2	3.78 [57]	1.3 [54]	0.5 [58]	0.58 [59]	9.2 [54]
GaAs	13.1 [60]	4.07 [60]	0.067 [60]	0.45 [60]	1.42 [60]

FIG. 3. (Color online) Plasma-supplied excess electron density n (upper panel) and the potential $-\phi$ (lower panel) it gives rise to, for a MgO surface in contact with a helium discharge with $n_0 = 10^7$ cm^{-3} and $k_B T_e = 2$ eV calculated without accounting for a SCR in the dielectric (crude ESL model). The cutoff of the interface region is $z_s = -z_0$. As can be seen, almost all of the plasma-induced wall charge is located in the well of the image potential in front of the surface.

the surface, but the minimum potential energy for electrons $-e\phi$ is reached inside the dielectric. Excess electrons coming from the plasma are thus mostly located inside the wall and the electron distribution extends deep into the bulk. This extended negative space charge also leads to a band bending near the surface. Note the different scales of the axes for the left and right panels of Fig. 4. On the scale where variations in the SCR are noticeable the ISR is basically a vertical line.

If one neglects the SCR and fills all excess electrons into the ISR (the crude ESL), the potential and the electron distribution
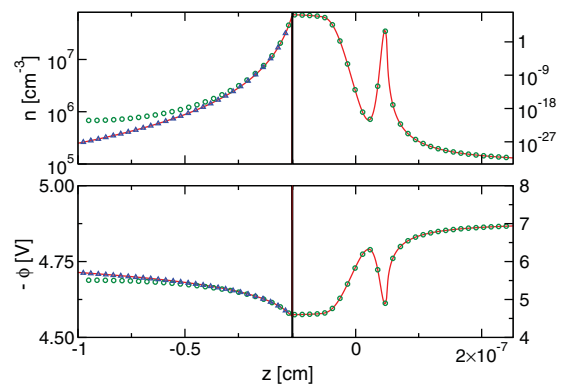

FIG. 4. (Color online) Plasma-supplied excess electron density n (upper panel) and the potential $-\phi$ (lower panel) it gives rise to, for an Al_2O_3 surface in contact with a helium discharge with $n_0 = 10^7$ cm^{-3} and $k_B T_e = 2$ eV. The red lines show data obtained from the refined ESL model accounting for an ISR and a SCR, the boundary between the two was put at $z_s = -3z_0$, the green circles show data for a model which consists only of an ISR with cutoff $z_s = -0.9$cm (crude ESL model), and the blue triangles show data for a model consisting only of a SCR for $z < 0$. Irrespective of the approximation, the plasma-induced wall charge extends deep into the bulk. Note the different scales of the axes for the left and right panels. On the spatial scale of the SCR shown in the left panels the ISR of the right panels becomes a vertical line.
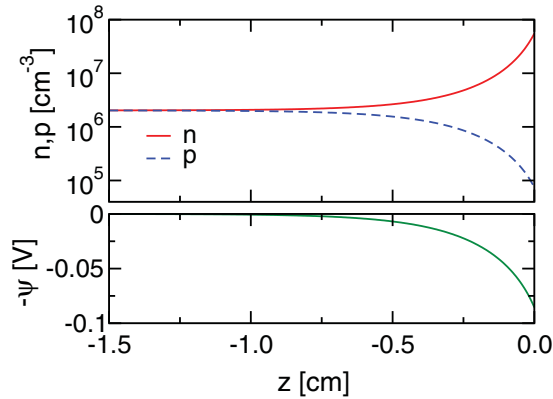
FIG. 5. (Color online) Electron density n and hole density p at a GaAs surface in contact with a helium discharge with $n_0 = 10^7 \mathrm{cm}^{-3}$ and $k_B T_e = 2$ eV calculated with the refined ESL model without ISR. The plasma-induced wall charge sits inside the GaAs wall. Deep inside the bulk charge neutrality is achieved by an equal density of electrons and holes.

are correctly described at and close to the surface but not far inside the dielectric (open green circles) because the *ad hoc* cutoff z_s of the crude ESL leads to an unphysical pileup of electrons near z_s. Hence, only if z_s is large enough does the crude ESL model give reliable results for the electron density and potential in the vicinity of the surface. Filling all electrons in the SCR, on the other hand, cannot describe the immediate vicinity of the surface correctly, which is however on the scale of the SCR an infinitesimally narrow region. It gives only for $z < -z_0$ a good description, that is, in the region where for $\chi > 0$ indeed most of the electrons are located (blue triangles).

While the crude ESL model containing only an ISR gives the correct electron density near the surface provided z_s is large enough, the merger of the ESL with the bulk can only be described with the refined ESL model including the SCR. This is particularly relevant for materials with smaller band gaps and larger intrinsic carrier concentrations than MgO, $\mathrm{Al_2O_3}$, and $\mathrm{SiO_2}$. To exemplify this we show in Fig. 5 the electron and hole densities (upper panel) as well as the potential $-\psi$ (lower panel) for a GaAs plasma wall, calculated for an ESL containing only a SCR. At the surface the electron density is about three orders of magnitude larger than the hole concentration. Thus, the gas phase plasma offers the possibility to manipulate the electron-hole plasmas by controlling the charge-carrier density—tantamount to doping—in the near surface region of a semiconductor. Deep inside the material, electron and hole concentrations are equal, leading to charge neutrality and a constant potential. The band bending due to the extended space charge in the ESL is about 0.09 eV.

Our results for the electron and hole densities and the potential in the dielectric depend of course on the model for the SCR. We have used for simplicity the model of an intrinsic semiconductor which is appropriate for an undoped semiconductor without impurities. Depending on doping or impurities a variety of models[42] could be used to take material-specific aspects into account. In our exploratory calculation we obtain a rather wide SCR. Including the effect of impurities, acting as trapping sites in the band gap would probably reduce the depth of the SCR considerably.
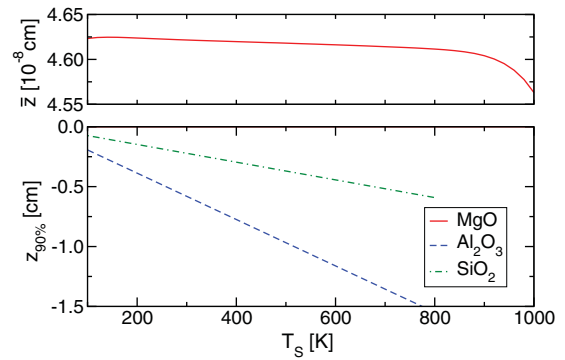

FIG. 6. (Color online) Center of gravity $\bar{z}$ of the plasma-supplied excess electron distribution at a MgO surface (upper panel) and the $z_{90\%}$ value for the electron distribution at an $\mathrm{Al_2O_3}$ and a $\mathrm{SiO_2}$ surface (lower panel), all in contact with a helium discharge with $n_0 = 10^7 \mathrm{cm}^{-3}$ and $k_B T_e = 2$ eV, as a function of the surface temperature T_S. The data shown in the upper and lower panel were obtained, respectively, from the crude ESL model and the refined ESL model without an ISR.

To summarize our results up to this point, we find that for negative electron affinity the plasma-induced electronic surface charge is located in front of the surface forming a quasi-two-dimensional electron gas, while for positive electron affinity the surplus electrons form a space-charge layer in the dielectric leading to a small bending of the energy bands.

The two distinct types of charge distributions in the ESL are also reflected in the dependence of the width of the plasma-supplied electron distribution on the surface temperature. Figure 6 shows the center of gravity $\bar{z}$ of the electron distribution for the MgO surface ($\chi < 0$) and the $z_{90\%}$ value for the surfaces of $\mathrm{Al_2O_3}$ and $\mathrm{SiO_2}$ ($\chi > 0$), where $z_{90\%}$ is implicitly defined by

$$\int_{z_{90\%}}^{0} dz[n(z) - p(z)] = 0.9N. \qquad (60)$$

We use the $z_{90\%}$ value because it captures the depth of the SCR better than $\bar{z}$, which depends too strongly on the few electrons that penetrate very deep into the bulk.

For negative electron affinity (MgO, shown in the upper panel of Fig. 6) the external surface charge is strongly trapped in the deep image potential so that $\bar{z}$ changes very little with surface temperature. The width of the internal surface charge for dielectrics with positive electron affinity ($\mathrm{Al_2O_3}$ and $\mathrm{SiO_2}$, lower panel), however, increases dramatically with surface temperature. This can be understood as follows. The restoring force from the positive ions in the sheath binds internal surface charges only weakly to the surface. With increasing surface temperature, however, high-lying states in the conduction band get more and more populated. Hence, some electrons have rather high kinetic energies, are thus less confined near the surface by the weak restoring force, and penetrate therefore deeper into the bulk. As a result, the $z_{90\%}$ value decreases strongly with surface temperature.

Let us now turn to the discussion of the influence of the electron temperature $k_B T_e$ and the plasma density n_0 on the properties of the ESL. These two parameters enter through the total surface density of electrons N depleting the sheath

TABLE II. Surface density of electrons in the ESL N, wall potential ϕ_W, plasma sheath ESL boundary z_0, and the $z_{90\%}$ value for SiO$_2$ in contact with a helium discharge with $k_B T_e = 2$ eV for different values of the plasma density n_0.

n_0 (10^6cm^{-3})	N (10^6cm^{-2})	ϕ_W (V)	z_0 (10^{-5}cm)	$z_{90\%}$ (cm)
10	4.38	−7.07	5.14	−0.222
20	6.20	−7.07	4.32	−0.157
50	9.80	−7.07	3.44	−0.099
100	13.9	−7.07	2.89	−0.070

TABLE III. Surface density of electrons in the ESL N, wall potential ϕ_W, plasma sheath ESL boundary z_0, and the $z_{90\%}$ value for SiO$_2$ in contact with a helium discharge at $n_0 = 10^7$cm^{-3} for different values of the electron temperature $k_B T_e$.

$k_B T_e$ (eV)	N (10^6cm^{-2})	ϕ_W (V)	z_0 (10^{-5}cm)	$z_{90\%}$ (cm)
0.5	2.19	−1.77	7.27	−0.444
1	3.10	−3.53	6.11	−0.314
2	4.38	−7.07	5.14	−0.222
5	6.93	−17.7	4.086	−0.140

and accumulating in the ESL. How $k_B T_e$ and n_0 affect the interface depends therefore on the sheath model and the model used for the interaction between plasma particles and the surface. For simplicity we have used a collisionless sheath model and assumed the surface to be a perfect absorber for plasma electrons and ions. The results for the properties of the ESL as a function of the plasma parameters are thus to be taken as only indicative.

The effect of a variation of n_0 and $k_B T_e$ is most significant for surfaces with positive electron affinity. Table II shows the effect of the plasma density n_0 for a SiO$_2$ surface. If n_0 increases, the boundary z_0 between sheath and ESL moves closer to the surface. This, however, does not affect the charge distribution much as most of the electrons occupy the SCR inside the dielectric (as shown in Fig. 4 for Al$_2$O$_3$). More important is the fact that an increase in n_0 leads to an increase of the total surface electron density N. This entails a stronger restoring force from the plasma sheath so that the potential well confining the space charge inside the dielectric becomes steeper and the electrons in the SCR of the ESL are shifted toward the surface; in other words, the $z_{90\%}$ value increases with n_0. Mathematically, the steeplelike shape of the electron distribution arises because a larger N leads through Eq. (57) to a larger η_s which makes the potential steeper at the surface so
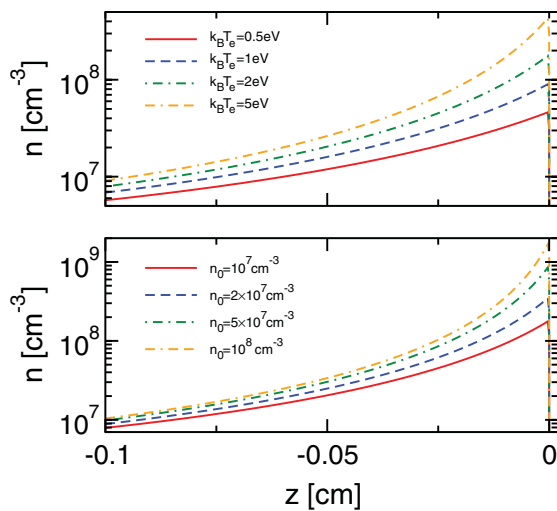

FIG. 7. (Color online) Plasma-supplied surplus electron density n at a SiO$_2$ surface in contact with a helium discharge as a function of the electron temperature (upper panel, $n_0 = 10^7$cm^{-3}) and the plasma density (lower panel, $k_B T_e = 2$ eV) for $T_S = 300$ K. The refined ESL model without an ISR was employed to produce the data.

that the electron distribution is more peaked there. This trend can be seen in the lower panel for Fig. 7.

A variation of the electron temperature $k_B T_e$ has similar effects as the variation of the plasma density. If $k_B T_e$ increases, the total surface density of electrons increases also, as can be seen from Table III. As shown in the upper panel of Fig. 7, this leads again to a steeplelike electron distribution which is more concentrated at the surface the higher the electron temperature is.

For a surface with negative electron affinity (MgO) the surplus electrons are strongly bound in the image potential. While a variation of $k_B T_e$ or n_0 changes the total number of surplus electrons per unit area in the same way as for a surface with positive electron affinity, the distribution of the surplus electrons within the ESL is not affected significantly because of the strong image interaction.

So far we have shown the potential and the electron distribution in the ESL. Now, we will compare potential and charge distribution in the ESL with the ones in the plasma sheath. The electron distribution at the interface is the quasistationary electron gas on top of the charge redistribution due to the truncation of the solid that guarantees flux equality at the sheath-ESL boundary z_0. As already mentioned, not included in this simple model is the flux of plasma electrons and ions in the ESL before the electrons are trapped at the surface and the ions recombine with the negative wall charge. The electron and ion densities in this model are thus discontinuous at z_0. The potential, however, which has been obtained from the integration of Poisson's equation is continuous and differentiable everywhere. Between the well of the image potential and z_0 the electron and ion flux from the sheath would be important. The neglect of the charge densities associated with these fluxes does however not affect the potential because they are too small to have a significant effect.

Figure 8 shows the ESL and the plasma sheath in front of a MgO surface. Due to the negative electron affinity, the plasma-supplied surface electrons are bound by the image potential in front of the surface. In Fig. 8, we plot the electron and ion density (upper panel), as well as the electric potential (lower panel) over the distance from the surface z. Far from the surface, the potential approaches the bulk plasma value chosen to be zero. In the sheath the potential develops a Coulomb barrier and reaches the wall potential ϕ_w at z_0, the distance where the sheath merges with the surface layer (vertical dotted line). The wall potential is the potential just outside to which the energies of the bulk states are referenced. Closer to the surface the potential follows the attractive image
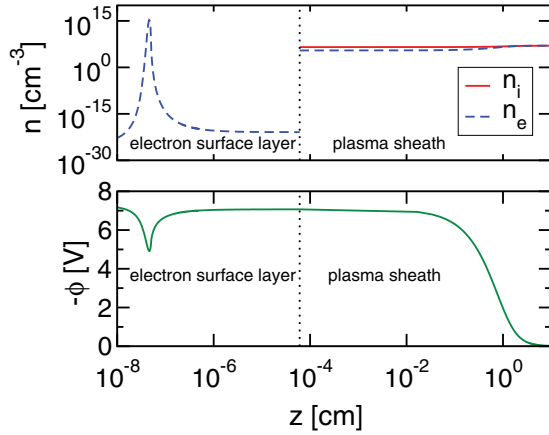
FIG. 8. (Color online) Density of plasma-supplied surplus electrons trapped in the ESL as well as electron and ion density in the plasma sheath (upper panel) and potential (lower panel) for a MgO surface in contact with a helium discharge ($n_0 = 10^7 \text{cm}^{-3}$ and $k_B T_e = 2$ eV). The data were obtained from the crude ESL model.

potential while at the surface the repulsive potential due to the negative electron affinity prevents the electron from entering the dielectric (only scarcely seen on the scale of the figure).

In Fig. 9 we finally plot the electron and ion densities (upper panel) as well as the electric potential (lower panel) for SiO$_2$. Note the linear z axis in contrast to the logarithmic z axis of Fig. 8. Due to the positive electron affinity, the excess electrons constituting the wall charge penetrate deep into the dielectric and occupy therefore the SCR of the ESL. Compared to the variation of the electric potential in the sheath the band bending in the dielectric induced by the wall charge is rather small, as indicated by the variation of ϕ inside the dielectric. This is because ϵ is large and the width of the SCR is narrow on the scale of the sheath. Only on the scale of the ISR (a vertical line at $z = 0$), the SCR of the ESL is wide.
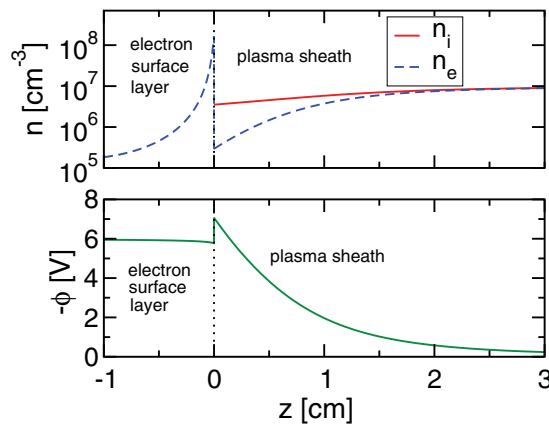

FIG. 9. (Color online) Density of plasma-supplied excess electrons in the ESL as well as electron and ion density in the plasma sheath (upper panel) and potential (lower panel) for a SiO$_2$ surface in contact with a helium discharge ($n_0 = 10^7 \text{cm}^{-3}$ and $k_B T_e = 2$ eV). The refined ESL model without an ISR was employed to produce the data.

V. CONCLUSIONS

We have studied the potential and the charge distribution across the interface of a plasma and a dielectric wall, treating the plasma-induced wall charge as a quasistationary electron gas trapped by and in thermal equilibrium with the dielectric. Our approach is based on a model for a graded surface including the offset between the potential just outside the dielectric and the conduction-band minimum arising from the redistribution of charge due to the truncation of the solid as well as the image potential due to the dielectric mismatch at the boundary. The missing electrons from the sheath populate the interface potential and thereby form an electron surface layer (ESL) which minimizes the grand canonical potential of wall-thermalized excess electrons and satisfies Poisson's equation.

Within this model the boundary between the plasma sheath and the ESL is given by the distance from the crystallographic interface where the potential for the excess electrons turns from the repulsive sheath potential into the attractive surface potential. This distance is typically on the order of a micron. It gives the position of an effective wall for plasma electrons and ions and thus of the portion of the ESL which lays in front of the surface. Most of the surplus electrons trapped in the ESL, that is, the plasma-induced wall charge, will be, however, much closer to the surface or even inside the dielectric depending on the electron affinity.

We presented numerical results for the potential and the distribution of the plasma-supplied surplus electrons at the interface between a helium discharge and the surfaces of MgO, Al$_2$O$_3$, and SiO$_2$, respectively. The electron distribution within the ESL strongly depends on the electron affinity. For negative electron affinity, the conduction-band minimum is above the potential just outside the dielectric. Hence, it is energetically unfavorable for electrons to penetrate into the bulk and the surface electrons are bound in the image potential in front of the surface. In this case, their spatial profiles change little over a variation of the surface temperature or the plasma parameters. For positive electron affinity the conduction-band minimum is below the potential just outside the dielectric and the surface-bound electrons accumulate inside the wall. The space charge in the bulk broadens if the surface temperature is increased and becomes more peaked if the total surface density of the electrons missing in the sheath is raised through an increase in either the plasma density or the electron temperature.

Separating the ESL into an interface-specific and a space-charge region and modeling the bulk of the dielectric as an intrinsic semiconductor, we also investigated how the ESL merges with the bulk of the dielectric. This is particularly important for dielectrics with small energy gaps and positive electron affinities, where excess electrons coming from the sheath accumulate not in the image potential in front of the surface but deep inside the wall. In this case the wall charge may also induce a significant band bending.

Whereas the crude ESL model we proposed neglects the space charge deep inside the bulk of the wall and is thus only applicable to large band-gap dielectrics with negative electron affinity, where basically the whole plasma-induced wall charge is trapped in the image potential in front of the

surface, the refined ESL model, keeping the interface-specific region as well as the space-charge region of the ESL, provides a quantitative description of the whole spatial structure of the extended charge double layer which forms at a dielectric plasma wall as a result of the electrons in the ESL and the positive space charge in the plasma sheath.

The ESL can be regarded as that part of the plasma sheath which is inside the plasma wall. It is thus the ultimate boundary of a bounded gas discharge and constitutes, depending on the electron affinity, either a quasi-two-dimensional electron plasma in front of the wall or an electron(-hole) plasma inside the wall.

[1] O. Ishihara, J. Phys. D: Appl. Phys. **40**, R121 (2007).

[2] V. E. Fortov, A. V. Ivlev, S. A. Khrapak, A. G. Khrapak, and G. E. Morfill, Phys. Rep. **421**, 1 (2005).

[3] D. A. Mendis, Plasma Sources Sci. Technol. **11**, A219 (2002).

[4] U. Kogelschatz, Plasma Chem. Plasma Process. **23**, 1 (2003).

[5] L. Stollenwerk, S. Amiranashvili, J.-P. Boeuf, and H.-G. Purwins, Phys. Rev. Lett. **96**, 255001 (2006).

[6] L. Stollenwerk, J. G. Laven, and H.-G. Purwins, Phys. Rev. Lett. **98**, 255001 (2007).

[7] R. Dussart *et al.*, Eur. Phys. J. D **60**, 601 (2010).

[8] C. J. Wagner, P. A. Tchertchian, and J. G. Eden, Appl. Phys. Lett. **97**, 134102 (2010).

[9] K. H. Becker, K. H. Schoenbach, and J. G. Eden, J. Phys. D: Appl. Phys. **39**, R55 (2006).

[10] N. P. Ostrom and J. G. Eden, Appl. Phys. Lett. **87**, 141101 (2005).

[11] M. J. Kushner, J. Phys. D: Appl. Phys. **38**, 1633 (2005).

[12] R. N. Franklin, *Plasma Phenomena in Gas Discharges* (Clarendon, Oxford, 1976).

[13] M. A. Lieberman and A. J. Lichtenberg, *Principles of Plasma Discharges and Materials Processing* (Wiley-Interscience, New York, 2005).

[14] K.-U. Riemann, J. Phys. D: Appl. Phys. **24**, 493 (1991).

[15] K. G. Emeleus and J. R. M. Coulter, Int. J. Electron. **62**, 225 (1987).

[16] K. G. Emeleus and J. R. M. Coulter, IEE Proceedings A Science Measurement and Technology **135**, 76 (1988).

[17] J. F. Behnke, T. Bindemann, H. Deutsch, and K. Becker, Contrib. Plasma Phys. **37**, 345 (1997).

[18] D. Uhrlandt, M. Schmidt, J. F. Behnke, and T. Bindemann, J. Phys. D: Appl. Phys. **33**, 2475 (2000).

[19] Y. B. Golubovskii, V. A. Maiorov, J. Behnke, and J. F. Behnke, J. Phys. D: Appl. Phys. **35**, 751 (2002).

[20] F. X. Bronold, H. Deutsch, and H. Fehske, Eur. Phys. J. D **54**, 519 (2009).

[21] R. L. Heinisch, F. X. Bronold, and H. Fehske, Phys. Rev. B **81**, 155420 (2010).

[22] R. L. Heinisch, F. X. Bronold, and H. Fehske, Phys. Rev. B **82**, 125408 (2010).

[23] F. X. Bronold, R. L. Heinisch, J. Marbach, and H. Fehske, IEEE Trans. Plasma Sci. **39**, 644 (2011).

[24] R. L. Heinisch, F. X. Bronold, and H. Fehske, Phys. Rev. B **83**, 195407 (2011).

[25] F. X. Bronold, H. Fehske, H. Kersten, and H. Deutsch, Phys. Rev. Lett. **101**, 175002 (2008).

[26] M. W. Cole and M. H. Cohen, Phys. Rev. Lett. **23**, 1238 (1969).

[27] B. Baumeier, P. Kruger, and J. Pollmann, Phys. Rev. B **76**, 205404 (2007).

[28] M. Rohlfing, N.-P. Wang, P. Kruger, and J. Pollmann, Phys. Rev. Lett. **91**, 256802 (2003).

[29] V. M. Silkin, J. Zhao, F. Guinea, E. V. Chulkov, P. M. Echenique, and H. Petek, Phys. Rev. B **80**, 121408(R) (2009).

[30] V. M. Silkin, E. V. Chulkov, and P. M. Echenique, Phys. Rev. B **60**, 7820 (1999).

[31] U. Hoefer, I. L. Shumay, C. Reuss, U. Thomann, W. Wallauer, and T. Fauster, Science **277**, 1480 (1997).

[32] T. Fauster, Appl. Phys. A **59**, 479 (1994).

[33] F. Stern, Phys. Rev. B **17**, 5009 (1978).

[34] F. Stern and S. DasSarma, Phys. Rev. B **30**, 840 (1984).

[35] J. Planelles and J. L. Movilla, Phys. Rev. B **73**, 235350 (2006).

[36] E. E. Tkharev and A. L. Danilyuk, Vacuum **35**, 183 (1985).

[37] N. D. Mermin, Phys. Rev. **137A**, 1441 (1965).

[38] W. Kohn and L. J. Sham, Phys. Rev. **140A**, 1133 (1965).

[39] R. O. Jones and O. Gunnarson, Rev. Mod. Phys. **61**, 689 (1989).

[40] P. J. Jennings, R. O. Jones, and M. Weinert, Phys. Rev. B **37**, 6113 (1988).

[41] A. V. Gavrilenko, C. S. McKinney, and V. I. Gavrilenko, Phys. Rev. B **82**, 155426 (2010).

[42] H. Lüth, *Solid Surfaces, Interfaces and Thin Films* (Springer-Verlag, Berlin, 1992).

[43] R. T. Tung, Mater. Sci. Eng. **R35**, 1 (2001).

[44] D. Cahen and A. Kahn, Adv. Mater. **15**, 271 (2003).

[45] F. J. Himpsel, J. A. Knapp, J. A. VanVechten, and D. E. Eastman, Phys. Rev. B **20**, 624 (1979).

[46] K. P. Loh, I. Sakaguchi, M. N. Gamo, S. Tagawa, T. Sugino, and T. Ando, Appl. Phys. Lett. **74**, 28 (1999).

[47] J. B. Cui, J. Ristein, and L. Ley, Phys. Rev. Lett. **81**, 429 (1998).

[48] F. Maier, J. Ristein, and L. Ley, Phys. Rev. B **64**, 165411 (2001).

[49] J. D. Jackson, *Classical Electrodynamics* (Wiley, New York, 1998).

[50] N. W. Ashcroft and N. D. Mermin, *Solid State Physics* (Saunders College Publ., Philadelphia, 1976).

[51] M. Wintersgill, J. Fontanella, C. Andeen, and D. Schuele, J. Appl. Phys. **50**, 8259 (1979).

[52] W. H. Butler, X.-G. Zhang, T. C. Schulthess, and J. M. MacLaren, Phys. Rev. B **63**, 054416 (2001).

[53] M. Schubert, T. E. Tiwald, and C. M. Herzinger, Phys. Rev. B **61**, 8187 (2000).

[54] E. Bersch, S. Rangan, R. A. Bartynski, E. Garfunkel, and E. Vescovo, Phys. Rev. B **78**, 085114 (2008).

[55] T. V. Perevalov, A. V. Shaposhnikov, V. A. Gritsenko, H. Wong, J. H. Han, and C. W. Kim, JETP Lett. **85**, 165 (2007).

[56] R. H. French, J. Am. Ceram. Soc. **73**, 477 (1990).

[57] Y. D. Glinka and M. Jaroniec, J. Appl. Phys. **82**, 3499 (1997).

[58] R. Ludeke, H. J. Wen, and A. Schenk, Appl. Phys. Lett. **73**, 1221 (1998).

[59] R. K. Chanana, J. Appl. Phys. **109**, 104508 (2011).

[60] B. van Zeghbroeck, *Principles of Semiconductor Devices and Heterojunctions* (Prentice-Hall, Upper Saddle River, 2010).